4.2 Global Spectral Model (JMA-GSM0603)

4.2.1 Introduction

The Global Spectral Model (GSM) employs the primitive equations to express the resolvable motions and states of the atmosphere. It also includes sophisticated parameterization schemes for physical processes. In the horizontal, prognostic variables are spectrally discretized with a truncation wave number of triangular 319 (T_L319). The corresponding transform grids are spaced by about 0.5625 degree in both longitude and latitude. In the vertical, the model places 40 layers up to 0.4 hPa.

GSM has been operational at JMA since March 1988. The model originally had a horizontal resolution of T63 and 16 vertical layers up to 10 hPa with a sigma-coordinate.

In November 1989, the model was upgraded. The truncation wave number and the number of vertical layers were increased to T106 and 21, respectively. A hybrid η vertical coordinate was adopted.

In March 1996, the horizontal resolution was doubled to T213. The number of vertical layers was also increased to 30. The cumulus parameterization was changed from a Kuo scheme to a prognostic Arakawa-Schubert scheme.

In December 1999, extensive refinement for the physical package was performed. Cloud water content started to be treated as a prognostic variable, and the moist convection process was improved.

In March 2001, the number of vertical layers was increased to 40 and the vertical domain was extended up to 0.4 hPa. The model was highly parallelized to suit a massively distributed-memory parallel computer.

In February 2005, an Eulerian advection scheme was replaced by a semi-Lagrangian one, with an increase in the spectral resolution from T213 (quadratic grid) to T_L319 (linear grid). An incremental non-linear normal mode initialization and a vertical mode initialization were also introduced.

On March 1st, 2006, operations at 06, 18UTC were started with forecast time of 36 hours in addition to 00UTC with 90 hours and 12UTC with 216 hours.

4.2.2 Dynamics

GSM has been constructed on the framework of semi-implicit semi-Lagrangian global model. The general shortcomings of semi-Lagrangian models are firstly the lack of conservation property and secondly the heavy cost of three-dimensional interpolations. In order to overcome these difficulties, Yoshimura and Matsumura (2003; 2004) has developed a vertically conservative semi-Lagrangian scheme, in which a vertical advection is treated separately from a horizontal advection so that the model may preserve the conservation of vertically integrated quantity such as water vapor under the non-dissipative condition. The separate treatment enables the model to reduce the cost of interpolations, as well as to recover the conservative property.

(a) Governing equations

GSM adopts an η vertical coordinate, which is a hybrid between pressure p and σ ($\sigma = p/p_S$, p_S is surface pressure), implicitly defined as $p = A(\eta)+B(\eta)p_S$. Prognostic variables, that is, wind vector $\mathbf{u}=(u, v)$, temperature T, pressure p, specific humidity q and cloud water content q_c obey the system of primitive equations in η-coordinates as follows:

$$\frac{d\mathbf{u}}{dt} \equiv \left(\frac{\partial}{\partial t} + \mathbf{u}\cdot\nabla + \dot{\eta}\frac{\partial}{\partial \eta} \right)\mathbf{u} = -f\mathbf{z}\times\mathbf{u} - \left(\nabla\Phi + R_d T_V \nabla \ln p\right) + \mathbf{F}_\mathbf{u} \tag{4.2.1}$$

$$\frac{dT}{dt} = \frac{\kappa T_V \omega}{\left[1+\left(C_{pv}/C_{pd}-1\right)q\right]p} + F_T \tag{4.2.2}$$

$$\frac{dq}{dt} = F_q \tag{4.2.3}$$

$$\frac{dq_c}{dt} = F_c \tag{4.2.4}$$

$$\frac{\partial}{\partial t}\frac{\partial p}{\partial \eta} + \nabla\cdot\left(\mathbf{u}\frac{\partial p}{\partial \eta}\right) + \frac{\partial}{\partial \eta}\left(\dot{\eta}\frac{\partial p}{\partial \eta}\right) = 0\,, \tag{4.2.5}$$

where d/dt and ∇ represents a total derivative and a horizontal gradient operator respectively. Integrating Eq. (4.2.5) with respect to η with the boundary condition $\dot{\eta} = 0$ at η=0 and η=1, η-velocity and ω are found:

$$\dot{\eta}\frac{\partial p}{\partial \eta} = -\frac{\partial p}{\partial t} - \int_0^\eta \nabla\cdot\left(\mathbf{u}\frac{\partial p}{\partial \eta}\right)d\eta\,, \tag{4.2.6}$$

$$\omega \equiv \frac{dp}{dt} = -\int_0^\eta \nabla\cdot\left(\mathbf{u}\frac{\partial p}{\partial \eta}\right)d\eta + \mathbf{u}\cdot\nabla p\,. \tag{4.2.7}$$

Geopotential Φ is given by the hydrostatic relation:

$$\frac{\partial\Phi}{\partial \eta} = -R_d T_v \frac{\partial \ln p}{\partial \eta}\quad. \tag{4.2.8}$$

The other notation used above is conventional: $\mathbf{z}$ is the unit vertical vector, T_v virtual temperature, f Coriolis parameter, R_d gas constant for dry air and $\kappa=R_d/C_{pd}$. C_{pd} and C_{pv} are the specific heat capacity at constant pressure of dry air and water vapor respectively. $\mathbf{F}_\mathbf{u}$, F_T, F_q and F_c are tendencies due to physical processes. In addition, $\mathbf{F}_\mathbf{u}$ and F_T include the effect of horizontal diffusions described in later.

(b) Vertical finite difference scheme

The vertical finite difference scheme is coded according to Simmons and Burridge (1981). The prognostic variables $\mathbf{u}$, T, q and q_c are defined on the full levels, while η (vertical fluxes as well) are on the half-integer levels. Pressure on the half-integer levels are expressed as

$$p_{k-1/2} = A_{k-1/2} + B_{k-1/2}p_S \qquad (k = 1,2,\ldots,\mathrm{kmax})\,, \tag{4.2.9}$$

here the level index k increases with height, and $A_{k-1/2} = A(\eta_{k-1/2})$, $B_{k-1/2} = B(\eta_{k-1/2})$. $A_{1/2}$ is set to zero so that the lowest level coincides with the ground surface. $B_{k-1/2}$ above 50 hPa are set to zero so that these levels coincide with constant pressure surfaces. For the intermediate levels, $A_{k-1/2}$ and $B_{k-1/2}$ vary smoothly and monotonically with k.

From the hydrostatic relation given by Eq. (4.2.8) the finite difference form of geopotential on the full level is chosen as

$$\Phi_k = \Phi_S + \sum_{k'=1}^{k-1} R_d T_{Vk'} \ln\left(\frac{p_{k'-1/2}}{p_{k'+1/2}}\right) + \alpha_k R_d T_{Vk}\,, \tag{4.2.10}$$

$$\alpha_k = \begin{cases} 1 - \dfrac{p_{k+1/2}}{\Delta p_k} \ln\dfrac{p_{k-1/2}}{p_{k+1/2}} & (1 \le k < \mathrm{kmax}) \\ \ln 2 & (k = \mathrm{kmax}) \end{cases}. \tag{4.2.11}$$

Then the pressure gradient force term in Eq. (4.2.1) and the adiabatic heating rate term in Eq. (4.2.2) can be written in discretized forms as

$$\begin{aligned} \left(\nabla\Phi + R_d T_V \nabla \ln p\right)_k &= \nabla\Phi_S + \left[\sum_{k'=1}^{k-1} R_d \nabla T_{Vk'} \ln\left(\frac{p_{k'-1/2}}{p_{k'+1/2}}\right) + \alpha_k R_d \nabla T_{Vk}\right] + h_k \nabla p_s \\ h_k &= \sum_{k'=1}^{k-1} R_d T_{Vk'} \left(\frac{B_{k'-1/2}}{p_{k'-1/2}} - \frac{B_{k'+1/2}}{p_{k'+1/2}}\right) + \frac{R_d T_{Vk}}{p_{k-1/2}} B_{k-1/2} \end{aligned}, \tag{4.2.12}$$

and

$$\left[\frac{\kappa T_V}{C_p / C_{pd}} \frac{\omega}{p}\right]_k = \frac{\kappa T_{Vk}}{C_{pk} / C_{pd}} \frac{1}{\Delta p_k} \left[\left(\ln\frac{p_{k-1/2}}{p_{k+1/2}}\right)\left(B_{k+1/2}\mathbf{u}_k \cdot \nabla p_S - \sum_{l=k+1}^{\mathrm{kmax}} \nabla\cdot\left(\mathbf{u}_l \Delta p_l\right)\right) - \alpha_k \left(\nabla\cdot\mathbf{u}_k\right)\Delta p_k\right], \tag{4.2.13}$$

respectively. Vertical mass flux in Eq. (4.2.6) is discretized as

$$\left(\dot\eta \frac{\partial p}{\partial \eta}\right)_{k-1/2} = -B_{k-1/2} \frac{\partial p_S}{\partial t} - \sum_{l=k}^{\mathrm{kmax}} \nabla\cdot\left(\mathbf{u}_l \Delta p_l\right) = B_{k-1/2} \sum_{l=1}^{\mathrm{kmax}} \nabla\cdot\left(\mathbf{u}_l \Delta p_l\right) - \sum_{l=k}^{\mathrm{kmax}} \nabla\cdot\left(\mathbf{u}_l \Delta p_l\right). \tag{4.2.14}$$

(c)Semi-implicit semi-Lagrangian formulation

Prior to the integration, forecast equations (4.2.1)-(4.2.4) are rewritten in the form of $d_H X/dt = R$ with the vertical advection terms incorporated into R on the right-hand sides. They are integrated with respect to t along the trajectory of the parcel from a departure point D at time $t-\Delta t$ to an arrival point A at time $t+\Delta t$. The linear term L separated from the forcing term R is treated semi-implicitly (i.e. by a trapezoidal rule), and the remaining R including vertical advection terms are treated with a spatial averaging (Tanguay et al. 1992).

The resulting linear terms are a little amplified by a factor β=1.2 for stability: finally we get

$$X^{A+} - X^{D-} = 2\Delta t \frac{R^{A0} + R^{D0}}{2} + 2\Delta t\beta\left[\frac{L^{A+} + L^{D-}}{2} - \frac{L^{A0} + L^{D0}}{2}\right]. \tag{4.2.15}$$

Superscript A represents an arrival point $\mathbf{x}_{ij}$ assuming just on the Gaussian grid, and D a departure point $\mathbf{x}_{ij}-\boldsymbol{\alpha}$, (the displacement vector $\boldsymbol{\alpha}$, how to calculate will be described later); the abbreviations used above are $X^{A+}=X(\mathbf{x}, t+\Delta t)$, $X^{D-}=X(\mathbf{x}-\boldsymbol{\alpha}, t-\Delta t)$, $R^{A0}=R(\mathbf{x}, t)$, $R^{D0}=R(\mathbf{x}-\boldsymbol{\alpha}, t)$ and so on. Rearranging terms in the above equations, we get a system of linear equations for the unknowns X^{A+}:

$$X^{A+} - \beta\Delta t L^{A+} = \left[X^{-} + R^{0}\Delta t - \beta\Delta t\left(L^{0} - L^{-}\right)\right]^{D} + \left[R^{0}\Delta t - \beta\Delta t L^{0}\right]^{A} \tag{4.2.16}$$

(d) Vertically conservative semi-Lagrangian scheme

Equations (4.2.16) would be reformulated in flux forms adequate for the scheme in which the vertical advection may retain a conservative property. Beginning with Eq. (4.2.5) and (4.2.1)-(4.2.4), they are rewritten as follows:

$$\frac{d_H}{dt}\frac{\partial p}{\partial \eta} = -D\frac{\partial p}{\partial \eta} - \frac{\partial}{\partial \eta}\left(\dot{\eta}\frac{\partial p}{\partial \eta}\right) \tag{4.2.17}$$

$$\frac{d_H}{dt}\left(X\frac{\partial p}{\partial \eta}\right) = -DX\frac{\partial p}{\partial \eta} - \frac{\partial}{\partial \eta}\left(\dot{\eta}X\frac{\partial p}{\partial \eta}\right) + R_X\frac{\partial p}{\partial \eta}, \tag{4.2.18}$$

where X stands for **u**, T_V, q and q_c, $R_X = dX/dt$. We notice at a glance that there is a parallelism between these equations. The first term of each right hand side of these equations represents the increase by horizontal convergence, and the second term the increase by vertical flux convergence. With respect to vertical flux convergence, q and q_c being conservative when $R_X = 0$, it may be promising to devise a vertically integrated quantity to be unchanged in the vertical advection. Here an outline of the procedure will be described simply in the case of specific humidity q without R_q.

Vertical discretization and time integration during 2Δt described earlier give the following equations with omitting terms related to semi-implicit method for simplicity:

$$\begin{aligned}\left(\Delta p_k\right)^{A+} = &\left[\left(\Delta p_k\right)^{-} - \left(D_k\Delta p_k\right)^{0}\Delta t + \left\{\left(\dot{\eta}\frac{\partial p}{\partial \eta}\right)_{k+1/2} - \left(\dot{\eta}\frac{\partial p}{\partial \eta}\right)_{k-1/2}\right\}^{0}\Delta t\right]^{D} \\ &+\left[-\left(D_k\Delta p_k\right)^{0}\Delta t + \left\{\left(\dot{\eta}\frac{\partial p}{\partial \eta}\right)_{k+1/2} - \left(\dot{\eta}\frac{\partial p}{\partial \eta}\right)_{k-1/2}\right\}^{0}\Delta t\right]^{A},\end{aligned} \tag{4.2.19}$$

$$\begin{aligned}\left(q_k\Delta p_k\right)^{A+} = &\left[q_k^{-}\left(\Delta p_k\right)^{-} - q_k^{-}\left(D_k\Delta p_k\right)^{0}\Delta t + \left\{\left(q\dot{\eta}\frac{\partial p}{\partial \eta}\right)_{k+1/2} - \left(q\dot{\eta}\frac{\partial p}{\partial \eta}\right)_{k-1/2}\right\}^{0}\Delta t\right]^{D} \\ &+\left[-q_k^{+}\left(D_k\Delta p_k\right)^{0}\Delta t + \left\{\left(q\dot{\eta}\frac{\partial p}{\partial \eta}\right)_{k+1/2} - \left(q\dot{\eta}\frac{\partial p}{\partial \eta}\right)_{k-1/2}\right\}^{0}\Delta t\right]^{A},\end{aligned} \tag{4.2.20}$$

$$p_{k-1/2} = \sum_{k'=k}^{\mathrm{kmax}}\Delta p_{k'}, \qquad (k = 1,2,\ldots,\mathrm{kmax}+1). \tag{4.2.21}$$

If we define a vertically cumulative quantity Q as follows:

$$Q_{k-1/2} = \sum_{k'=k}^{\mathrm{kmax}}\Delta Q_{k'}, \quad \Delta Q_k = q_k\Delta p_k \quad (k = 1,2,\ldots,\mathrm{kmax}+1) \quad , \tag{4.2.22}$$

then it is found that Eq. (4.2.20) rewritten for ΔQ_k is similar to (4.2.19) for Δp_k and that there is clear correspondence between Q and p. We can, therefore, carry out a computation of Q step by step in the following five steps in a parallel fashion to p. The first two steps concern operations inside of the square bracket $[\ldots]^{\mathrm{D}}$ in the above equations. The third step is the calculation of variables at the departure points by an interpolation. The fourth and the fifth step proceed in

the similar way to the first two steps but in the bracket $[\ldots]^{A}$.

(i) The first step: compute the horizontal divergence; as the mass of each layers Δp_k vary to $\Delta p_k'$, half level pressures $p_{k-1/2}$, which the layers are bounded by, also shift to $p_{k-1/2}'$ that can be computed by Eq. (4.2.21). While q_k remain constant under the horizontal convergence: $q_k' = q_k$.

(ii) The second step: calculate the vertical flux convergence using Eq. (4.2.14) which is the same as in Eulerian scheme; in the same way as the first step, $\Delta p_k'$ vary to $\Delta p_k''$, and $p_{k-1/2}'$ shift to $p_{k-1/2}''$ except k=1 ($p_{1/2}' = p_{1/2}''$). In this step, the shift of $Q_{k-1/2}'$ due to the vertical flux convergence are computed by the interpolation from $Q_{k-1/2}'(p_{k-1/2}')$ using $Q_{k-1/2}'' = Q_{k-1/2}'(p_{k-1/2}'')$. This procedure ensures the conservation of total mass-weighted integral $Q_{1/2}' = Q_{1/2}''$, because $p_{1/2}' = p_{1/2}''$ holds and the other $p_{k-1/2}''$(k=2,3,…kmax) merely change their intervals in the vertical column. New q_k'' are computed from $\Delta Q_k''$ and $\Delta p_k''$ by Eq. (4.2.22).

(iii)The third step: take horizontal advection into account with computing $(\Delta p_k)^{D}$ and q_k^{D} by quasi-cubic interpolation.

(iv)The forth and (v)the last step: proceed with calculation in reverse order to the steps prior to the horizontal advection; that is, at the first comes the evaluation of vertical flux convergence, the second of horizontal divergence.

Through these five steps the time-integration of q and q_c are completed, while that of the other **u**, T_V and p_S are followed by the semi-implicit calculation shown in Eq. (4.2.16).

(e)Determination of a departure point

Displacement vector **α,** which remains undetermined as yet, obeys the following implicit equation $\boldsymbol{\alpha} = 2\Delta t\left(\mathbf{u}_k(\mathbf{x}_{ij} - \boldsymbol{\alpha}, t) + \mathbf{u}_k(\mathbf{x}_{ij}, t)\right)/2$ that states the horizontal advection during the time interval 2Δt is caused by the average wind of two endpoints of the trajectory. This implicit equation is solved by successive insertions of **α.** On computing of these vector components, we take into account that the axes of the local coordinates (λ, φ) rotate due to the spherical metric as a parcel advances along a trajectory, as is the case whenever horizontal vector components would be interpolated on the sphere. The wind at the departure point is computed by a linear interpolation except for the last third iteration by a quasi-cubic.

(f) Spectral method and a horizontal diffusion

Spectral variables, that is, vorticity $\zeta(=\mathbf{z}\cdot\nabla\times\mathbf{u})$, divergence $D(=\nabla\cdot\mathbf{u})$, T_V and $\ln(p_S)$ are expanded in terms of the spherical harmonics with a triangular truncation. In accordance with the framework of semi-Lagrangian scheme, a linear Gaussian transformation grid is used. Solving the semi-implicit equations, calculation of the horizontal diffusion and such as the differentials on the sphere, are performed by the spectral method (Bourke, 1974; Hoskins and Simmons, 1975). The remaining variables q and q_c are defined only on the grid points.

In order to prevent the accumulation of small scale noises (spectral blockings), fourth-order linear horizontal diffusion is applied to ζ, D and T_V backward implicitly in the spectral forms at the independent step after the semi-implicit calculation:

$$\left(\frac{\partial \zeta}{\partial t}\right)_{hdiff} = -K\left(\nabla^4 - \frac{4}{a^4}\right)\zeta \tag{4.2.23a}$$

$$\left(\frac{\partial D}{\partial t}\right)_{hdiff} = -K_D \nabla^4 D \tag{4.2.23b}$$

$$\left(\frac{\partial T_V}{\partial t}\right)_{hdiff} = -K\nabla^4\left[T_V - \frac{\partial \overline{T}_V}{\partial \overline{p}}\, p\right] = -K\nabla^4\left[T_V - \frac{\partial \overline{T}_V}{\partial \overline{p}}\, B(\eta) p_S\right], \tag{4.2.23c}$$

where K and K_D are horizontal diffusion coefficients. The bar over a variable indicates global average on η-surface. The angular momentum conservation does not allow the horizontal diffusion process to work on the vorticity with total wave number 1 as shown in Eq. (4.2.23a). Diffusion for virtual temperature is modified so as to work on the constant pressure surface; otherwise the diffusion on the declined η-surface may produce spurious mixings along steep mountain slopes. The diffusion coefficients are chosen so that the power spectrum of enstrophy coincides with that expected from the 2-dimensional turbulence theory, though K_D is doubled for the sake of computational stability. In the layers above 100hPa, the coefficients are gradually enhanced with height so as to simulate a sponge layer that absorbs the waves incident upon an upper boundary. A Rayleigh damping for the temperature deviation from the global average on η-surface is also implemented to the highest three layers with 10 to 20 days relaxation times.

4.2.3 Radiation

The radiative heating rate is computed as the convergence of the net radiation fluxes F;

$$\left(\frac{\partial T}{\partial t}\right)_{rad} = \frac{g}{C_p}\frac{\partial F}{\partial p}, \tag{4.2.24}$$

where g is the acceleration of gravity and C_p is the specific heat at constant pressure of moist air. The solution of the radiative transfer equation is computationally very expensive. In order to cut down on the computational costs, the full radiation computations for longwave and shortwave are only done every three hours and hourly, respectively, on a coarser (reduced radiation) grid.

(a) Longwave radiation

The basic framework of the longwave fluxes and cooling rates computations follows Chou et al. (2001). Longwave radiation is treated by a broad-band flux emissivity method for nine spectral bands shown in Fig. 4.2.1.

Assuming a non-scattering atmosphere, the net longwave radiation flux F can be given by

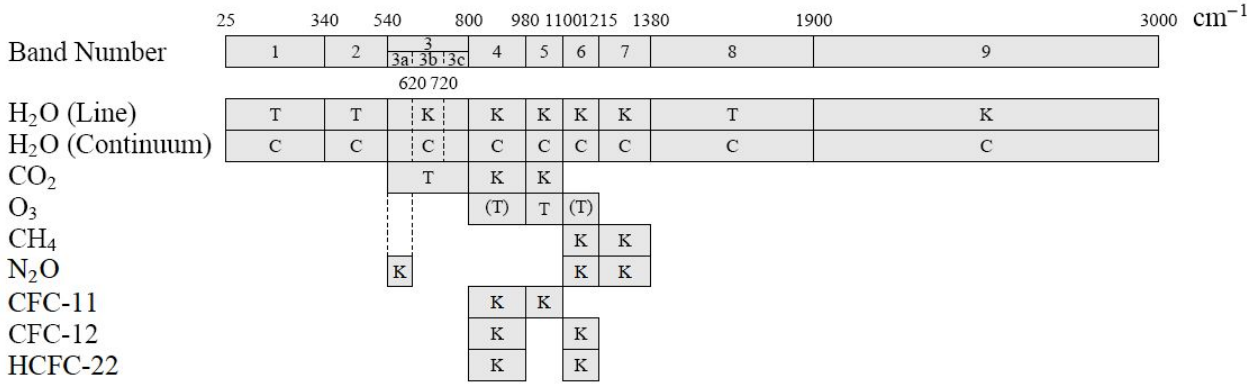

Fig. 4.2.1 Spectral regions for evaluation of broad-band transmissivities. Letters in the figure represent methods for calculating transmittance; K: k-distribution method, T: table look-up method, C: parameterization of water vapor continuum absorption.

$$F(p) = C(p, p_{bottom})\left[\pi B(T_{ground}) - \pi B(T_{bottom})\right]\tau(p, p_{bottom}) + \int_{p_{top}}^{p_{bottom}} C(p, p')\,\tau(p, p')\,\frac{\partial \pi B(T')}{\partial p'}\,dp' , \qquad (4.2.25)$$

where $\tau(p, p')$ is the band transmissivity between p and p', and $B(T)$ the total Planck function. $C(p, p')$ is the clear sky fraction between p and p' derived from the fractional cloud covers with the assumption of maximum-random cloud overlap proposed by Geleyn and Hollingsworth (1979). Clouds are treated as blackbodies, so that the effective cloudiness of semi-transparent cloud is given by the product of the horizontal coverage by the emissivity.

The band transmissivity is normalized by the Planck function $B_\nu(T)$ for each absorber in a given spectral region $\Delta\nu$:

$$\tau(p, p') = \int_{\Delta\nu} B_\nu(T_0)\tau_\nu(p, p')d\nu \Big/ \int_{\Delta\nu} B_\nu(T_0)d\nu , \qquad (4.2.26)$$

where T_0 is 250 K. Depending on the absorber and the spectral band, the band transmissivities are evaluated with three different approaches: a pre-computed table look-up method (Chou and Kouvaris, 1991) and a k-distribution method (Arking and Grossmann, 1972) for line absorption, and a parameterization for water vapor continuum absorption. Absorption data of gases are derived from HITRAN2000 (Rothman et al., 2003) for water vapor, carbon dioxide, ozone, methane, nitrous oxide and 3 CFCs. The e-type and P-type continuum absorptions by water vapor are treated after the method of Zhong and Haigh (1995) with some refinements. Considering the Doppler broadening effect of the lines in the k-distribution method, absorption coefficient is adjusted by a pressure scaling technique based on Line-by-Line calculation. The diffusivity factor of 1.66 is used to approximate the integration over the direction of the radiance transmission.

(b) Shortwave radiation

Shortwave scattering and absorption are modeled by a two-stream formulation using the delta-Eddington approximation (Joseph et al., 1976 and Coakley et al., 1983). The spectrum is divided into 22 bands based on Freidenreich and Ramaswamy (1999), except that water vapor in a near-infrared region is based on Briegleb (1992). Assuming a plane parallel atmosphere, the diffuse radiance I is governed by the radiation transfer equation

$$\mu \frac{dI}{d\delta} + I = \frac{\omega_0}{2} \int_{-1}^{+1} p(\mu, \mu') I(\delta, \mu') d\mu' + \frac{\omega_0}{2} S_0 \, p(\mu, \mu_0) \exp(-\frac{\delta}{\mu_0}) , \tag{4.2.27}$$

where δ and ω_0 are the optical thickness and the single scattering albedo, respectively, and S_0 the incident solar irradiance in the direction μ_0 (the cosine of the solar zenith angle). The scattering phase function $p(\mu, \mu')$ defines the probability that radiation coming from direction μ' is scattered in direction μ. In the delta-Eddington method, the phase function is approximated by a two-term expansion of the phase function with a forward-scatter peak f;

$$p(\mu, \mu') = 2f \, \delta(\mu - \mu') + (1 - f)(1 + 3\frac{g - f}{1 - f} \mu \mu') , \tag{4.2.28}$$

where $\delta(\mu - \mu')$ is the Dirac delta function and g the asymmetry factor.

Considering an atmosphere where a fraction C_{total}, which depends on the cloud overlap assumption, is covered by clouds, the final fluxes are given as a weighted average of the fluxes in the cloudy and clear sky fractions of the column:

$$F = C_{total} F_{cloudy} + (1 - C_{total}) F_{clear-sky} . \tag{4.2.29}$$

The reflectance and transmittance of the cloudy and clear sky fraction of the layer are calculated as functions of the total optical thickness δ_{total}, the total single scattering albedo $\omega_{0\,total}$ and the total asymmetry factor g_{total} of the layer,

$$\begin{aligned} \delta_{total} &= \delta_R + \delta_g + \delta_a + \delta_c , \\ \omega_{0\,total} &= \frac{\delta_R + \omega_{0a}\delta_a + \omega_{0c}\delta_c}{\delta_R + \delta_g + \delta_a + \delta_c} , \\ g_{total} &= \frac{g_a \omega_{0a} \delta_a + g_c \omega_{0c} \delta_c}{\delta_R + \omega_{0a}\delta_a + \omega_{0c}\delta_c} , \end{aligned} \tag{4.2.30}$$

where the subscripts ‘ R ’, ‘ g ’, ‘ a ’ and ‘ c ’ denote the molecular Rayleigh scattering, the gaseous absorptions, and the Mie scattering/absorption due to aerosols and cloud droplets, respectively.

The cloud optical properties are parameterized as functions of the cloud water path CWP and the droplet radius;

$$\delta_c = CWP(a + b/r_e),$$
$$\omega_{0c} = c + dr_e, \tag{4.2.31}$$
$$g_c = e + fr_e,$$

where the coefficients $a,\ldots,f$ are specified differently for the liquid droplets (Slingo, 1989) and for the ice particles (Ebert and Curry, 1992), and r_e is the effective radius of the liquid droplets and ice particles (see below).

(c) Radiatively active constituents

Radiatively active gases are prognostic water vapor, climatological ozone, globally uniform carbon dioxide (at 375ppmv), oxygen (at 209490ppmv), methane (at 1.75ppmv), nitrous oxide (at 0.28ppmv) and CFC-11, CFC-12, HCFC-22 (at 0.3, 0.5, 0.2ppbv, respectively). The monthly mean concentrations of ozone are specified from a 3-dimensional Chemical Transport Model calculation. The concentration and optical properties of aerosols are specified as the continental and maritime types of background values without seasonal variation. The cloud fraction and water content are provided from the cloud scheme. The effective radius of the cloud liquid droplets is fixed at 13 and 10 micrometers over the ocean and the land, respectively. The effective radius of the ice crystals varies depending on cloud temperature and cloud ice content (Wyser, 1998).

4.2.4 Cumulus convection

(a) Cumulus model

An economical version of the Arakawa - Schubert scheme (Arakawa and Schubert, 1974) developed at JMA is implemented. For an economical computation, two simplifications are introduced. First, the vertical profile of the upward mass flux η is assumed to be a linear function of height z, as proposed by Moorthi and Suarez (1992), in the following way; $\eta=1+\lambda(z - z_b)$, where λ denotes the entrainment rate and z_b is the cloud base height. Secondly, the mass flux at the cloud base is determined by solving a prognostic equation (Randall and Pan, 1993) rather than by applying the quasi-equilibrium assumption. The cloud base level is fixed near 900hPa in the model. The moist static energy and other thermodynamic properties of the upward mass flux at the cloud base are given by the grid-scale values at the maximum moist static energy level below the cloud base.

Following the concept of Arakawa and Schubert (1974), we consider the ensemble effect of multiple-type cumuli. Each type is defined by the level of the cloud top, where the updraft cloud mass loses its buoyancy and the detrainment occurs. During the upward movement of the cloud air mass, the entrainment of the environment air mass is considered. The entrainment rate λ of each cumulus is determined from the no buoyancy condition at the cloud top. An upper limit of λ is set to $1\text{x}10^{-3}$ m^{-1}.

We assume all the condensed water in the updraft is carried up to the cloud top. A part of the condensed water falls into the environment as rainwater, while the remaining is detrained as cloud water. The ratio of rainwater and cloud

water is linearly changed with the cloud depth. The cloud water is redistributed to the layer whose temperature is below the freezing point.

(b) Upward mass flux

The following prognostic equation is used for the upward mass flux at the cloud base M_B;

$$\frac{dM_B(\lambda)}{dt} = \max\left[\frac{A(\lambda) - f\,A_0(\lambda)}{2\alpha}, 0\right] \min\left[\frac{\lambda}{\lambda_{\min}}, 1\right] - \frac{M_B(\lambda)}{2\tau_d} \tag{4.2.32}$$

where A denotes the cloud work function, A_0 denotes the average of observed cloud work functions given by Lord and Arakawa (1980), and τ_d denotes the time constant of cumulus kinetic energy decay. A parameter f is introduced to include effects of grid-scale vertical wind and convective inhibition. It is given by;

$$f = \frac{\omega}{\omega_0} + \frac{A_i}{A_{i0}} + c \tag{4.2.33}$$

where ω denotes the vertical pressure velocity, A_i denotes the work for lifting the parcel to the level of free convection and ω_0, A_{i0} and c are empirically determined constants. In order to suppress tall cumuli in a dry condition and to include the effect of the turbulence in the planetary boundary layer, the parameter $\lambda_{\min}$ is defined as follows;

$$\lambda_{\min} = \max\left[\frac{0.9 - RH}{0.2}, 10^{-3}\right] \times \frac{0.3}{l_0} \tag{4.2.34}$$

where RH denotes the vertical mean of the relative humidity between cloud base and cloud top and l_0 denotes the mixing length of the planetary boundary layer.

(c) Convective downdraft

The convective downdraft associated with the cumulus affects the environment through the reduction of the net upward mass flux and the detrainment from the downdraft. For an economical reason, only one type of downdraft is assumed, while many types are considered in the updraft scheme.

The downdraft is initiated at the level where the net upward mass flux is reduced to half value of that at the cloud base. The downdraft mass flux M_d at the cloud base is given by

$$M_d = 0.4\, M_B \tag{4.2.35}$$

The entrainment from the environment is assumed to occur above the cloud base, while the detrainment to occur both above and below the cloud base. The entrainment rate and the detrainment rate are set to the same constant value above the cloud base.

(d) Mid-level convection

In the extratropics, moist convections do not always arise from the top of the planetary boundary layer. The mid-level convection scheme is incorporated to represent cumulus convection with its roots in the free atmosphere. The cloud base of the mid-level convection is given by the level of the largest moist static energy in the vertical column. The cloud top is defined as the level where the air mass lifted from the cloud base with constant entrainment rate loses its buoyancy. The upward mass flux at the cloud base is given by

$$\frac{dM_B}{dt} = \frac{A}{2\alpha} - \frac{M_B}{2\tau_d} \tag{4.2.36}$$

where A denotes the cloud work function.

(e) Convective momentum transport

The parameterization of the convective momentum transport follows the scheme proposed by Kershaw and Gregory (1997) and Gregory et al. (1997). The horizontal momentum tendency due to convection is parameterized as

$$\frac{\partial(\rho \bar{\boldsymbol{v}})}{\partial t} = -\frac{\partial M_u}{\partial z}\bar{\boldsymbol{v}}^u + \frac{\partial}{\partial z}(M_u \bar{\boldsymbol{v}}) + \frac{\partial M_d}{\partial z}\bar{\boldsymbol{v}}^d - \frac{\partial}{\partial z}(M_d \bar{\boldsymbol{v}}) \tag{4.2.37}$$

where $\boldsymbol{v}$ is the horizontal component of the wind, ρ is the air density, M_u and M_d are the upward and downward mass fluxes. The overbar denotes an average over the horizontal grid and the superscript u (d) denotes a contribution from the convective upward (downward) domain. The entrainment and detrainment are assumed to occur between cloud base and cloud top.

(f) Effects on the large scale tendency

The effects of the cumulus convection on the large scale tendency are calculated through large scale budget equations. The major contributions of the cumulus convection are made through 1) the compensating downward motion, 2) the detrainment of moisture from updraft at the cloud top, 3) the detrainment from convective downdraft and 4) convective momentum transport.

4.2.5 Clouds and large-scale precipitation

Clouds are prognostically determined in a similar fashion to that of Smith (1990). A simple statistical approach proposed by Sommeria and Deardorff (1977) is adopted for the calculation of the cloud amount and the cloud water content. In each grid box, the total moisture (water vapor and cloud water) and the liquid water temperature are

assumed to vary within the grid box due to unresolved atmospheric fluctuations with a uniform probability distribution. The cloud fraction C is given by the part of the grid box where the total moisture q_w exceeds the saturation specific humidity q_s,

$$C = \frac{\overline{q}_w + \Delta q_w - q_s}{2\Delta q_w} \tag{4.2.38}$$

where Δq_w is the maximum local deviation from the grid-box mean total moisture $\overline{q}_w$. In this regard, to form marine stratocumulus clouds, the cloud fraction C is diagnosed by the following scheme proposed by Kawai and Inoue (2006) when specific conditions are met,

$$C = 12.0\left(-\frac{\partial\theta}{\partial p} - 0.07\right) \tag{4.2.39}$$

where θ is the potential temperature and p is the pressure. Liquid (ice) cloud is assumed when the temperature is above 0 deg C (below −15 deg C). Between −15 deg C and 0 deg C, mixed phase cloud exists and the mixing ratio is linearly changed with the temperature.

The parameterization of the conversion rate P from cloud water q_c to precipitation follows the scheme proposed by Sundqvist (1978),

$$P = c_0 q_c \left[1 - \exp\left\{-\left(\frac{q_c}{q_c^{crit}}\right)^2\right\}\right] \tag{4.2.40}$$

where $1/c_0$ represents a characteristic time scale of the conversion of cloud droplets into raindrops and q_c^{crit} is a critical cloud water content at which the release of precipitation becomes efficient. The coalescence process (collection of cloud droplets by raindrops falling through a cloud) and the Bergeron-Findeisen effect (enhancement of precipitation release in clouds containing a mixture of droplets and ice crystals) are modeled following Sundqvist et al. (1989).

Following Kessler (1969) and Tiedtke (1993), the evaporation rate E of the large-scale precipitation is parameterized as

$$E = b \times \frac{1}{\tau_e} \times (q_s - q) \times \left\{\left(\frac{p}{p_s}\right)^{1/2} \frac{1}{b}\frac{P_l}{P_{l0}}\right\}^{0.577} \tag{4.2.41}$$

where b is the clear-sky precipitation fraction (fixed at 0.5), q_s the saturation specific humidity, p is the pressure, p_s is the surface pressure and P_l is the local precipitation rate. The values of constants are $1/\tau_e$=5.44x10^{-4} s^{-1} and P_{l0}=5.9x10^{-3} kg m^{-2} s^{-1}. The melting process and the sedimentation of snow are also considered.

4.2.6 Surface turbulent fluxes

The surface turbulent fluxes are formulated as the bulk formulae following the Monin-Obukhov similarity theory,

$$\overline{(w'\mathbf{v}')}_s = -C_m|\mathbf{v}_1|\mathbf{v}_1 \tag{4.2.42}$$

$$\overline{(w'\theta')}_s = -C_h|\mathbf{v}_1|(\theta_1 - \theta_s) \tag{4.2.43}$$

$$\overline{(w'q')}_s = -C_h|\mathbf{v}_1|(q_1 - q_s) \tag{4.2.44}$$

where $\mathbf{v} = (u, v)$ is the horizontal wind, θ the potential temperature and q the specific humidity, and subscripts "1" and "s" indicate the variables at the lowest η level and at the ground surface, respectively.

The bulk Richardson number R_{iB} is defined as

$$R_{iB} = \frac{gz_1(\theta_{v1} - \theta_{vs})}{T_1|\mathbf{v}_1|^2} \tag{4.2.45}$$

where z_1 is the height of the lowest η level above the ground, θ_v the virtual potential temperature.

Using the stability functions proposed by Louis et al. (1982), the drag coefficients can be written as follows;

$$C_m = \begin{cases} \dfrac{\gamma_m}{1+10R_{iB}/\sqrt{1+5R_{iB}}} & R_{iB} > 0 \\ \gamma_m\left[1 - \dfrac{10R_{iB}}{1+75\gamma_m\sqrt{z_1|R_{iB}|/z_{0m}}}\right] & R_{iB} \le 0 \end{cases} \tag{4.2.46}$$

$$C_h = \begin{cases} \dfrac{\gamma_h}{1+15R_{iB}\sqrt{1+5R_{iB}}} & R_{iB} > 0 \\ \gamma_h\left[1 - \dfrac{15R_{iB}}{1+75\gamma_h\sqrt{z_1|R_{iB}|/z_{0h}}}\right] & R_{iB} \le 0 \end{cases} \tag{4.2.47}$$

$$\gamma_m = \frac{k^2}{\ln(z_1/z_{0m})\ln(z_1/z_{0m})}$$
$$\gamma_h = \frac{k^2}{\ln(z_1/z_{0m})\ln(z_1/z_{0h})} \tag{4.2.48}$$

where k is the von Kármán constant (=0.4) and $z_{0m,h}$ the surface roughness lengths.

Over the land, the surface roughness lengths ($z_{0m} = z_{0h}$) are determined from the vegetation types and are altered by the snow cover. Over the ocean, the surface wind stress depends on the oceanic waves excited by the surface winds, and the roughness length and wind-induced stress are iteratively calculated in the model. Following the method of Beljaars (1995), the surface roughness lengths over ice-free ocean are obtained by the Charnock (1955) relation,

$$z_{0m} = \frac{0.11\nu}{u_*} + \frac{\alpha}{g} u_*^{\,2}$$
$$z_{0h} = \frac{0.62\nu}{u_*} \tag{4.2.49}$$

where $u_* (\equiv \sqrt{-\overline{(w'\mathbf{v}')_s}})$ is the friction velocity, ν the kinematic viscosity of air (=1.5x10^{-5} m^2/s) and α the Charnock coefficient (=0.020). The surface roughness length over sea ice is fixed at 0.001m.

4.2.7 Vertical turbulent diffusion

The level 2 turbulence closure scheme of Mellor and Yamada (1974) is used to represent the vertical diffusion of momentum, heat and moisture. Based on the local-K theory, the turbulent transports are expressed as

$$\overline{w'\mathbf{v}'} = -K_m \frac{\partial \mathbf{v}}{\partial z} \tag{4.2.50}$$

$$\overline{w's_L{}'} = -K_h \frac{\partial s_L}{\partial z} \tag{4.2.51}$$

$$\overline{w'q_w{}'} = -K_h \frac{\partial q_w}{\partial z} \tag{4.2.52}$$

where $s_L (\equiv C_p T + gz - Lq_c)$ is the liquid water static energy and $q_w (\equiv q + q_c)$ the total water content.

Following the mixing-length theory, the diffusion coefficients can be written as

$$K_m = l^2 \left|\frac{\partial \mathbf{v}}{\partial z}\right| f_m(R_i) \tag{4.2.53}$$

$$K_h = l^2 \left|\frac{\partial \mathbf{v}}{\partial z}\right| f_h(R_i) \tag{4.2.54}$$

where the mixing length l is given according to Blackadar (1962),

$$l = \frac{kz}{1 + kz/l_0} \tag{4.2.55}$$

The asymptotic mixing length l_0 is determined from the sub-grid scale orographic variances and the planetary boundary layer depth.

The gradient Richardson number R_i is defined after the method of Smith (1990),

$$R_i = g\left\{\widetilde{\beta}_S \frac{\partial s_L}{\partial z} + \widetilde{\beta}_Q \frac{\partial q_w}{\partial z}\right\} \Big/ \left|\frac{\partial \mathbf{v}}{\partial z}\right|^2 \tag{4.2.56}$$

where $\widetilde{\beta}_S$ and $\widetilde{\beta}_Q$ are the buoyancy parameters in terms of the cloud-conserved quantities s_L and q_w, respectively. The stability functions f_m and f_h are given by Mellor and Yamada (1982).

4.2.8 Gravity wave drag

The parameterization for the orographic gravity wave drag consists of two components; one for long waves (wavelength >100km) and the other for short waves (wavelength ≈ 10 km). The long waves are assumed to propagate upward until reaching wave-breaking levels mainly in the stratosphere and exert drag there (type A scheme), while short waves are always regarded as trapped and dissipated within the troposphere (type B scheme). Therefore the fundamental difference between the two schemes appears in the vertical distribution of the momentum deposit. The type A scheme is based on Palmer et al. (1986) with some modifications. Details are explained in Iwasaki et al. (1989).

In both schemes, the momentum flux $\vec{\tau}_r$ excited by subgrid-scale variances of topography is determined by

$$\vec{\tau}_r = \min\left(C_{gw}\,\rho_r\,N_r\,v_r\,\sigma^2\,,\,\left|\vec{\tau}_{r,sat}\right|\right)\mathbf{v}_r/v_r \tag{4.2.57}$$

where

$$\vec{\tau}_{r,sat} = C_{gw}\,\rho_r\,N_r\,v_r\left(\frac{v_r}{2F_cN_r}\right)^2\mathbf{v}_r/v_r \tag{4.2.58}$$

C_{gw} is constant, ρ air density, N Brunt-Vaisala frequency, F_c critical Froude number and $v=|\mathbf{v}|$. The subscript r denotes the reference level where the gravity wave stresses (momentum fluxes) are generated. There is a maximum of the momentum flux due to the valley blocking phenomena. The valley blocking is caused by stagnant flows near bottoms of valleys, which are separated from flows in the free atmosphere above. This phenomenon occurs when the Froude number is below a critical value. The blocking effectively reduces the amplitudes of gravity waves. The topographic variances σ^2 are derived from the GTOPO30, which is 30"x30" geographical data. First, the mean elevation (h_m) and its standard deviation (σ_m) over a 5'x5' grid box are evaluated from GTOPO30. The standard deviation of (h_m–h) in a gaussian grid box is regarded as σ in the type A scheme where h denotes the elevation spectrally truncated at the model resolution, while the average of σ_m in the gaussian grid box is regarded as σ in the type B scheme.

In the type A scheme, the momentum deposit is determined by the amplitude saturation hypothesis. The gravity wave stress at the (k+1/2)-th level is given by

$$\vec{\tau}_{k+1/2} = \min\left(\left|\vec{\tau}_{k-1/2}\right|, \left|\vec{\tau}_{sat}\right|\right) \vec{\tau}_r / \left|\vec{\tau}_r\right| \tag{4.2.59}$$

where

$$\vec{\tau}_{sat} = C_{gw}\, \rho\, N\left(\mathbf{v} \cdot \frac{\vec{\tau}_r}{\left|\vec{\tau}_r\right|}\right)\left[\frac{\varepsilon}{2F_c N}\left(\mathbf{v} \cdot \frac{\vec{\tau}_r}{\left|\vec{\tau}_r\right|}\right)\right]^2 \frac{\vec{\tau}_r}{\left|\vec{\tau}_r\right|} \tag{4.2.60}$$

ε is a function of the Richardson number

$$R_i = N^2 \Bigg/ \left[\frac{\partial}{\partial z}\left(\mathbf{v} \cdot \frac{\vec{\tau}_r}{\left|\vec{\tau}_r\right|}\right)\right]^2 \tag{4.2.61}$$

The wave stress of short gravity waves decreases with altitude due to nonhydrostatic effects (e.g., Wurtele et al., 1987). In the type B scheme, the wave stress is simply assumed to be a quadratic function of pressure and to vanish around 700 hPa as follows:

$$\vec{\tau}(p) = \begin{cases} \vec{\tau}(p_s) \cdot \dfrac{(p/p_s - 0.7)^2}{0.3^2} & (p/p_s \geq 0.7) \\ 0 & (p/p_s < 0.7) \end{cases} \tag{4.2.62}$$

4.2.9 Land surface processes

The Simple Biosphere scheme (SiB) developed by Sellers et al. (1986) and Sato et al. (1989a,b) is implemented in the model. The evapotranspiration from dry leaves considerably reduces the Bowen ratio in the bright daytime. Fig. 4.2.2 shows heat and water flows in the analogy of an electric circuit.

Governing equations of the canopy temperature T_c, the ground surface temperature T_g, and the deep soil temperature T_d are

$$C_c \frac{\partial T_c}{\partial t} = R_c^n - H_c - LE_c \tag{4.2.63}$$

$$C_g \frac{\partial T_g}{\partial t} = R_g^n - H_g - LE_g - \frac{2\pi C_g}{\tau_D}(T_g - T_d) \tag{4.2.64}$$

$$\frac{\partial T_d}{\partial t} = \frac{2\pi}{\sqrt{365}\tau_D}(T_d - T_g) \tag{4.2.65}$$

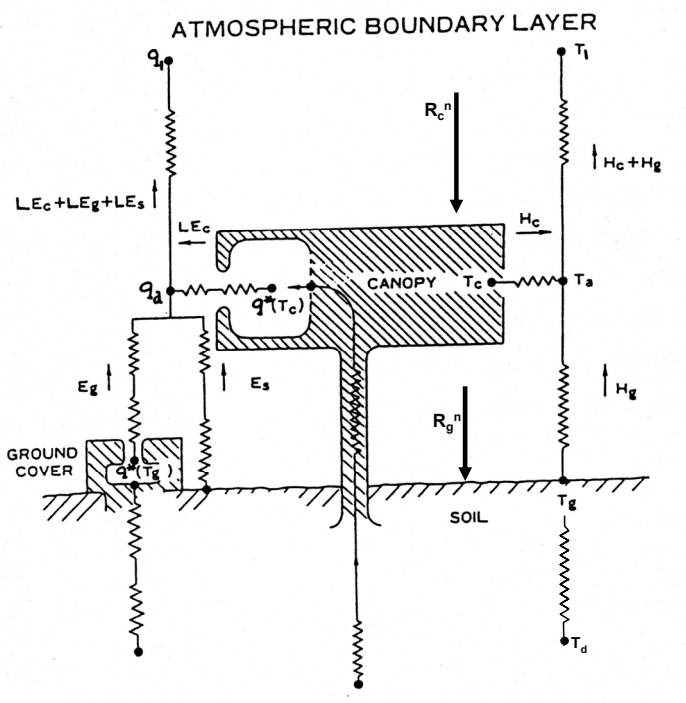

Fig. 4.2.2 Schematic illustration of the Simple Biosphere model (SiB). Temperature T_a and specific humidity q_a of the canopy space are related to the values at the lowest η level of the model by the surface boundary layer scheme.

where C is the heat capacity, R^n net radiation, H sensible heat, E evapotranspiration rate, L heat of evaporation, and τ_D the length of the day. The suffixes 'c', 'g' and 'd' denotes the canopy, the ground/ground grass and the deep soil, respectively. T_d is predicted with the force restore method (Deardorff, 1978). The initial conditions of T_c, T_g, T_d are given by those of the first guess, the 6-hour forecast initiated 6 hours before.

Water storage on leaves of the canopy (M_c) and the ground grass (M_g) are predicted by

$$\frac{\partial M_c}{\partial t} = P_c - D_c - \frac{E_{wc}}{\rho_w} \tag{4.2.66}$$

$$\frac{\partial M_g}{\partial t} = P_g - D_g - \frac{E_{wg}}{\rho_w} \tag{4.2.67}$$

where P represents precipitation over the leaves, D water drainage from the leaves, E_w evaporation of leaf-stored liquid water and ρ_w water density. When T_c (T_g) is less than the freezing point, M_c (M_g) represents ice on the canopy leaves (snow water equivalent).

The soil moisture W is predicted in three layers. Vegetation draws water from the soil and transfers it to the air directly. In this relation, the stomatal resistance, which depends on the leaf temperature and the intensity of solar radiation, considerably controls the evapotranspiration. Prognostic equations of the soil moisture in each layer are given as follows;

$$\frac{\partial W_1}{\partial t} = \frac{1}{\delta_s D_1}\left\{P_1 - Q_{1,2} - \frac{1}{\rho_w}\left(E_s + E_{dc,1} + E_{dg,1}\right)\right\} \tag{4.2.68}$$

$$\frac{\partial W_2}{\partial t} = \frac{1}{\delta_s D_2}\left\{Q_{1,2} - Q_{2,3} - \frac{1}{\rho_w}\left(E_{dc,2} + E_{dg,2}\right)\right\} \tag{4.2.69}$$

$$\frac{\partial W_3}{\partial t} = \frac{1}{\delta_s D_3}\left\{Q_{2,3} - Q_3\right\} \tag{4.2.70}$$

where P_1 is the infiltration of precipitation, $Q_{i,j}$ the water flux due to matric potential difference between i-th and j-th soil layer, Q_3 gravitational drainage, E_s evaporation from the bare soil, $E_{dc,i}$ drawn water from the i-th soil layer by the canopy transpiration, and $E_{dg,i}$ that by the ground grass transpiration. The surface overflow and the gravitational drainage of water are counted as the run-off Q_r,

$$Q_r = P_0 - P_1 + Q_3 \tag{4.2.71}$$

where

$$P_0 = P - \left(P_c + P_g\right) + \left(D_c + D_g\right) \tag{4.2.72}$$

P is the total precipitation over the canopy and P_0 is the effective one over the bare soil. P_1 is limited due to the hydraulic conductivity of saturated soil. The initial condition of soil moisture is specified with the climatological data by Willmott et al. (1985). The snow depth provided by the Snow Depth Analysis (see 3.9) is used as the initial value of snow water equivalent M_g, with the assumption of constant snow density, 200 kg/m^3.

SiB is connected to the surface boundary layer scheme through the temperature T_a and specific humidity q_a of the canopy space. Vegetation types in the SiB scheme determine the surface roughness lengths.

4.2.10 Parallelization

GSM (TL319) is operationally executed with 16 nodes, relatively small number of elements of SR11000-J1, to perform 84-hour forecast within about 5.5 minutes of wall clock. The strategies for parallelization are 1) a simple structure is preferable, 2) instruction loads should be well balanced among nodes, and 3) reproducibility must be guaranteed even if the number of nodes changes. Therefore one-dimensional decomposition in cyclic order is adopted.

Fig. 4.2.3 shows the schematic design of the parallelization. The variable array is decomposed by latitudes in grid

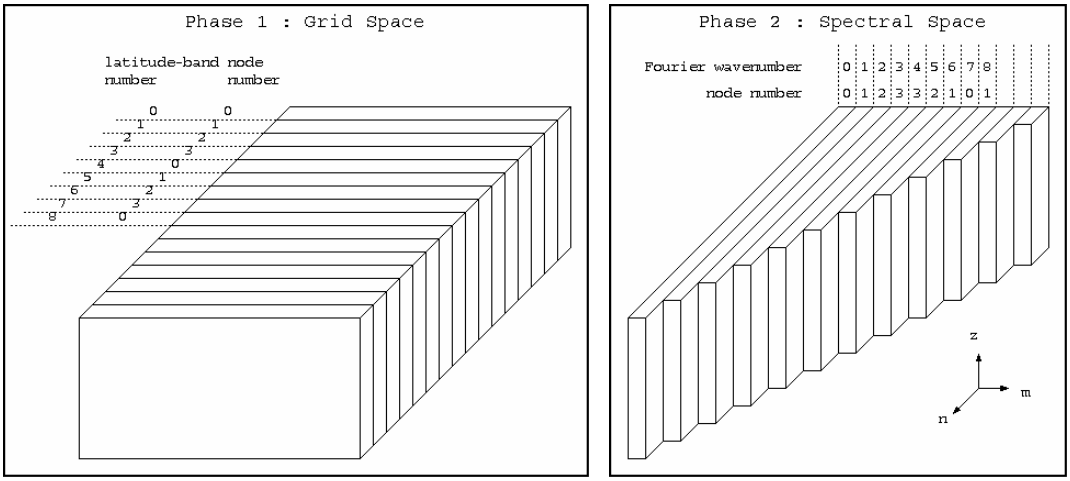

Fig. 4.2.3 Schematic design of the parallelization.

The number of nodes used is assumed to be 4 in this example.

space and by zonal wave numbers in spectral space so that all values needed for the summation in both Fourier and Legendre transformations are localized in a node. The cyclic decomposition in grid space is carried out in a symmetric manner with respect to the equator. It mitigates load imbalances associated with the physical parameterizations, since their computational loads depend mainly on land-sea distribution and latitudinal zones. It also reduces the computational cost of the Legendre transformation in which the symmetric/anti-symmetric properties of the associate Legendre functions are utilized. The cyclic decomposition in the spectral space is applied in such a way that the order of nodes reverses alternately. It is intended to mitigate the load imbalances related to the triangular truncation, in which the number of spectral components decreases with an increase of the zonal wave number.

4.2.11 Surface boundary conditions

The model topography is derived from the GTOPO30. The land-sea distribution is determined by referring to the Global Land Cover Characteristics (GLCC) database that is compiled by the U.S. Geological Survey (USGS) and others. The vegetation types are obtained from Dorman and Sellers (1989).

The analyzed anomaly of the sea surface temperature (SST) at the initial time is added to the seasonally changing climatological SST (Reynolds and Smith, 1994) during the time integration of the model. A sea area where the climatological sea ice concentration exceeds 55 % is regarded as a sea ice area (Nomura, 1998), which also changes gradually during the time integration of the model.

4.2.12 Initial conditions

The initial conditions for Zonal Wind, meridional wind, temperature, specific humidity and surface pressure are provided by the 4D-Var global objective analysis (see 3.5). The initial conditions for cloud water content, convective mass flux, canopy temperature, ground surface temperature and deep soil temperature are given by those of the first guess. The analyzed snow depth is used for determining the initial snow water equivalent as well as for adjusting the initial ground surface temperature.

4.2.13 Nonlinear normal mode initialization

Nonlinear normal mode initialization (NMI) including all physical processes is carried out in order to suppress high frequency gravitational oscillations caused by the initial imbalances between mass and wind fields. In order to avoid the large memory storage required for the normal modes of the high-resolution forecast model and preserving the atmospheric tidal oscillations, both an incremental and a vertical mode initialization scheme are simultaneously implemented (Murakami and Matsumura 2006).

In the incremental initialization (Ballish et al. 1992), Machenhauer's balance condition is imposed on the analysis increments not on the analysis itself. This is equivalent to adjust the tendency of the gravitational mode not to zero but to the values of that in the background fields of the analysis. Using Machenhauer's original NMI, the tidal oscillation disappears in the initial fields and shows spin-up in the course of the forecast unless the tendency of tidal oscillation is available in NMI-step independently of the scheme itself. In the incremental method, the tendency of tidal oscillation is given through the background fields instead of prescribed tidal fields under the condition that the tidal oscillation is well reproduced in the background fields of the analysis.

Vertical mode initialization has been devised for a *limited area* model (Bourke and McGregor 1983). It serves to save the computer memory because there is no need for the horizontal normal modes of a high-resolution *global* forecast model. As is well known, the horizontal normal modes are solutions to the horizontal structure equations which are identical to the linearized shallow water equations on the sphere with an equivalent depth determined from the vertical structure equation. Making the Coriolis parameters fixed at 60°N, the linearized vorticity and divergence equations on the sphere are derived. In these equations, the spherical harmonics, spanning the spectral base of the forecast model, remain uncoupled with each other and each of them constructs the spatial part of normal mode bases by itself.

The amplitude of each normal mode a_n is iteratively calculated as follows:

$$a_{n+1} = a_n - \frac{\dot{a}_n - \dot{b}}{i\omega} \tag{4.2.73}$$

where $\dot{a}_n$ and $\dot{b}$ are tendencies of each normal mode and that of background fields respectively, and ω is the eigen-frequency of the mode. This procedure is applied to the fast modes with the equivalent depth of the deepest five

and at the same time with the eigen-periods shorter than 9 hours.

4.2.14 Forecast performance

Fig. 4.2.4 shows RMSE for 500 hPa geopotential height against analysis in the northern hemisphere extratropics. Upper panel corresponds 24 hour forecast, middle and lower panels are 72 and 120 hour respectively. Dashed lines indicate the monthly means and solid lines represent 13 month moving averages. Substantial improvements are seen every time the model is upgraded (see 4.2.1).

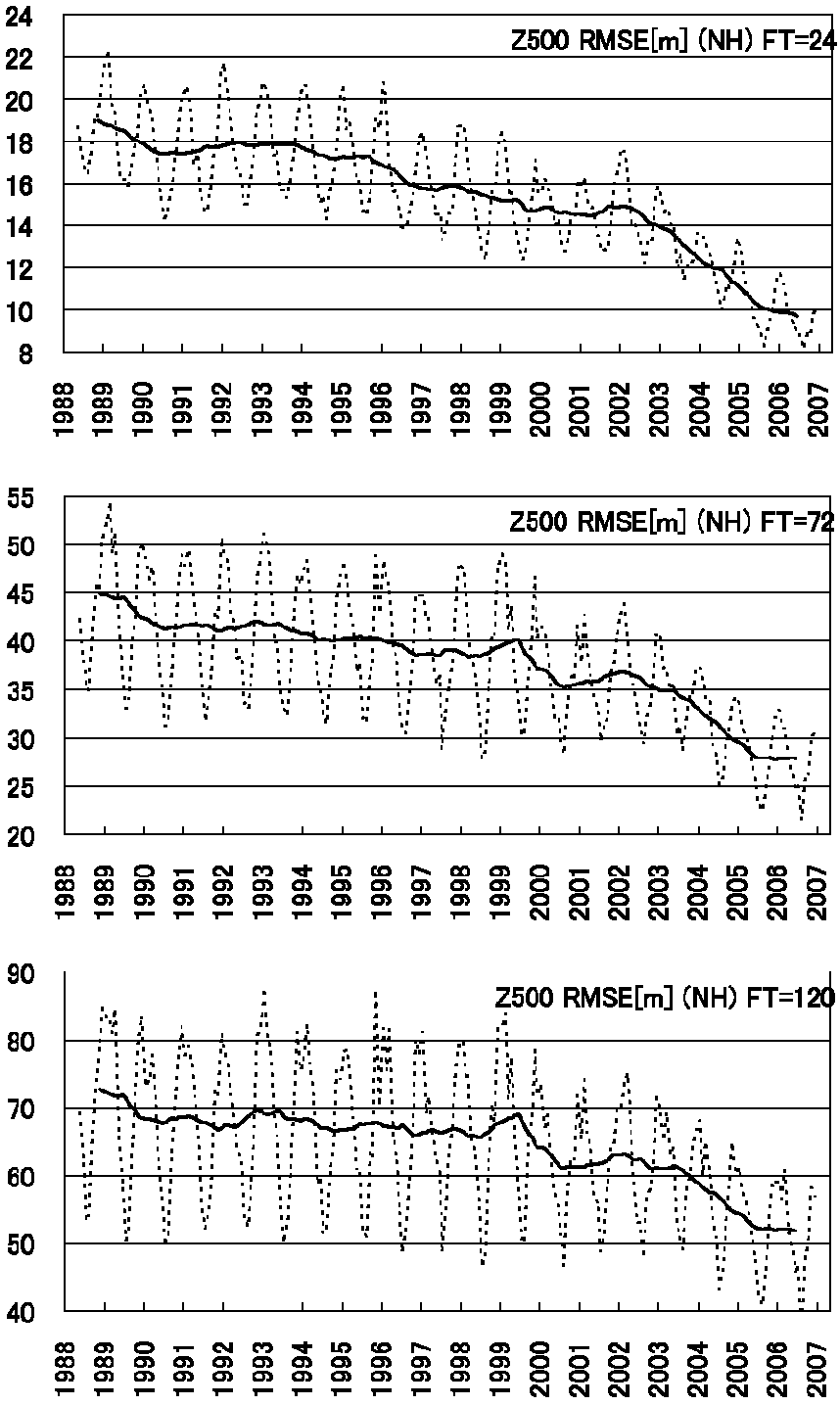

Fig. 4.2.4 Z500 RMSE against analysis in northern hemisphere extratropics (20N-90N). FT=24 (upper), 72 (middle) and 120 (lower) respectively. Dashed lines indicate monthly mean, thick solid lines 13 month moving average.

References

Arakawa, A. and W.H. Schubert, 1974: Interaction of a cumulus cloud ensemble with the large–scale environment, Part I. *J. Atmos. Sci.*, **31**, 674–701.

Arking, A.A. and K. Grossman, 1972: The influence of line shape and band structure on temperatures in planetary atmospheres. *J. Atmos. Sci.*, **29**, 937–949.

Ballish, B., X. Cao, E. Kalnay, and M. Kanamitsu, 1992: Incremental nonlinear normal-mode initialization. *Mon. Wea. Rev*., **120**, 1723–1734.

Beljaars, A.C.M., 1995: The parameterization of surface fluxes in large-scale models under free convection. *Q. J. R. Meteorol. Soc.*, **121**, 255–270.

Blackadar, A.K., 1962: The vertical distribution of wind and turbulent exchange in a neutral atmosphere. *J. Geophys. Res.*, **67**, 3095–3102.

Briegleb, B.P, 1992: Delta-Eddington Approximation for Solar Radiation in the NCAR Community Climate Model. *J. Geophys. Res.*, **97**, 7603–7612.

Bourke, W., 1974: A multi-level spectral model. I. Formulation and hemispheric integration. *Mon. Wea. Rev.*, **102**, 687–701.

Bourke, W. and J.L. McGregor, 1983: A Nonlinear vertical mode initialization scheme for a limited area prediction model. *Mon. Wea. Rev*., **111**, 2285–2297.

Charnock, H., 1955: Wind stress on a water surface. *Quart. J. Roy. Meteor. Soc.*, **81**, 639–640.

Chou, M.D. and L. Kouvaris, 1991: Calculations of transmission functions in the IR CO_2 and O_3 bands. *J. Geophys. Res.*, **96**, 9003–9012.

Chou, M.D., M.J. Suarez, X.Z. Liang, and M. M.-H. Yan, 2001: A thermal infrared radiation parameterization for atmospheric studies. Technical report series on global modeling and data assimilation Volume **19**, NASA Goddard Space Flight Center.

Coakley, J.A., R.D. Cess, and F.B. Yurevich, 1983: The effect of tropospheric aerosols on the earth's radiation budget: a parameterization for climate models. *J. Atmos. Sci.*, **40**, 116–138.

Deadorff, J.W., 1978: Efficient prediction of ground surface temperature and moisture with inclusion of a layer of vegetation. *J. Geophys. Res.*, **83**, 1889–1903.

Dorman, J. and P.J. Sellers, 1989: A global climatology of albedo, roughness length and stomatal resistances for atmospheric general circulation models as represented by the Simple Biosphere model (SiB). *J. Appl. Meteor.*, **28**, 833–855.

Ebert, E.E. and J.A. Curry, 1992: A parameterization of ice cloud optical properties for climate models. *J. Geophys. Res.*, **97**, 3831–3836.

Freidenreich, S.M. and V. Ramaswamy, 1999: A new multiple-band solar radiative parameterization for general circulation models. *J. Geophys. Res.*, **104**, 31389–31409.

Geleyn, J.-F. and A. Hollingsworth, 1979: An economical analytical method for the computation of the interaction

between scattering and line absorption of radiation. *Beitr. Phys. Atmos.*, **52**, 1–16.

Gregory, D., R. Kershaw and P.M. Inness, 1997: Parameterization of momentum transport by convection. II: Tests in single-column and general circulation models. *Quart. J. Roy. Meteor. Soc.*, **123**, 1153–1183.

Hoskins, B.J. and A.J. Simmons, 1975: A multi-layer spectral model and semi-implicit method. *Quart. J. Roy. Meteor. Soc.*, **101**, 637–655.

Iwasaki, T., S. Yamada, and K. Tada, 1989: A parameterization scheme of orographic gravity wave drag with two different vertical partitionings, part 1: Impact on medium range forecasts. *J. Meteor. Soc. Japan*, **67**,11–41.

Joseph, J.H., W.J. Wiscombe, and J.A. Weinman, 1976: The delta-Eddington approximation for radiative flux transfer. *J. Atmos. Sci.*, **33**, 2452–2459.

Kawai, H. and T. Inoue, 2006: A Simple Parameterization Scheme for Subtropical Marine Stratocumulus. *SOLA*, **2**, 017–020.

Kershaw, R. and D. Gregory, 1997: Parameterization of momentum transport by convection. I: Theory and cloud modelling results. *Quart. J. Roy. Meteor. Soc.*, **123**, 1133–1151.

Kessler, E., 1969: On the distribution and continuity of water substance in atmospheric circulation. *Meteorol. Monogr.*, **10**, American Meteorol. Soc., Boston, MA, 84pp.

Lord, S.J. and A. Arakawa, 1980: Interaction of a cumulus cloud ensemble with the large–scale environment. Part II. *J. Atmos. Sci.*, **37**, 2677–2692.

Louis, J.F., M. Tiedtke, and J.-F. Geleyn, 1982: 'A short history of the PBL parameterization at ECMWF'. Workshop on planetary boundary layer parameterization, November 1981, ECMWF, Reading, England.

Mellor, G. L. and T. Yamada, 1974: A hierarchy of turbulence closure models for planetary boundary layers. *J. Atmos. Sci.*, **31**, 1791–1806.

Mellor, G.L. and T. Yamada, 1982: Development of a turbulence closure model for geophysical fluid problems. *Rev. Geophys. Space Phys.*, **20**, 851–875.

Moorthi, S. and M.J. Suarez: 1992: Relaxed Arakawa–Schubert: A parameterization of moist convection for general circulation models. *Mon. Wea. Rev.*, **120**, 978–1002.

Murakami, H. and T. Matsumura, 2007: Development of an effective non-linear normal-mode initialization method for a high-resolution global model. *J. Meteor. Soc. Japan*, accepted.

Nomura, A., 1998: Global sea ice concentration data set used in ERA. *ECMWF Re–Analysis Project Series* vol. **4**, ECMWF.

Palmer, T.N., G.J. Schutts, and R. Swinbank, 1986: Alleviation of a systematic westerly bias in general circulation and numerical weather prediction models through an orographic gravity wave drag parametrization. *Quart. J. Roy. Meteor. Soc.*, **112**, 1001–1039.

Randall, D. and D.-M. Pan, 1993: Implementation of the Arakawa–Schubert cumulus parameterization with a prognostic closure. *Meteorological Monograph/The representation of cumulus convection in numerical models*., **46**, 137–144.

Reynolds, R.W. and T.M. Smith, 1994: Improved global sea surface temperature analyses using optimum interpolation.

J. Climate, **7**, 929–948.

Rothman, L.S., A. Barbe, D.C. Benner, L.R. Brown, C.Camy-Peyret, M.R. Carleer, K. Chance, C. Clerbaux, V. Dana, V.M. Devi, A. Fayt, J.-M. Flaud, R.R. Gamache, A. Goldman, D. Jacquemart, K.W. Jucks, W.J. Lafferty, J.-Y. Mandin, S.T. Massie, V. Nemtchinov, D.A. Newnham, A. Perrin, C.P. Rinsland, J. Schroeder, K.M. Smith, M.A. H. Smith, K. Tang, R.A. Toth, J. Vander Auwera, P. Varanasi, and K. Yoshino, 2003: The HITRAN molecular spectroscopic database: edition of 2000 including updates through 2001. *J. Quant. Spectrosc. Radiat. Transfer*, **82**, 5–44.

Sato, N., P.J. Sellers, D.A. Randall, E.K. Schneider, J. Shukla, J.L. Kinter III, Y–T Hou, and E. Albertazzi, 1989: Implementing the simple biosphere model (SiB) in a general circulation model: Methodologies and results. *NASA contractor Rep.*, **185509**, 76pp.

Sato, N., P.J. Sellers, D.A. Randall, E.K. Schneider, J. Shukla, J.L. Kinter III, Y–T Hou, and E. Albertazzi, 1989: Effects of implementing the simple biosphere model (SiB) in a general circulation model. *J. Atmos. Sci.*, **46**, 2757–2782.

Sellers, P.J., Y. Mintz, Y.C. Sud, and A. Dalcher, 1986: A simple biosphere model (SiB) for use within general circulation models. *J. Atmos. Sci.*, **43**, 505–531.

Simmons, A.J. and D.M. Burridge, 1981: An energy and angular momentum conserving vertical finite difference scheme and hybrid vertical coordinates. *Mon. Wea. Rev.*, **109**, 758–766.

Slingo, J., 1989: A GCM parameterization for the short wave radiative properties of water cloud. *J. Atmos. Sci.*, 46, 1419–1427.

Smith, R.N.B., 1990: A scheme for predicting layer clouds and their water content in a general circulation model. *Q. J. R. Meteorol. Soc.*, **116**, 435-460.

Sommeria, G. and J.W. Deardorff, 1977: Subgrid-scale condensation in models of nonprecipitating clouds. *J. Atmos. Sci.*, **34**, 344–355.

Sundqvist, H., 1978: A parameterization scheme for non-convective condensation including prediction of cloud water content. *Q. J. R. Meteorol. Soc.*, **104**, 677–690.

Sundqvist, H., E. Berge, and J.E. Kristjánsson, 1989: Condensation and cloud parameterization studies with a mesoscale numerical weather prediction model. *Mon. Wea. Rev.*, **117**, 1641–1657.

Tanguay, M., E. Yakimiw, H. Ritchie, and A. Robert, 1992: Advantage of spatial averaging in semi-implicit semi-Lagrangian schemes. *Mon. Wea. Rev*., **120**, 113–123.

Tiedtke, M., 1993: Representation of Clouds in Large-Scale Models. *Mon. Wea. Rev.*, **121**, 3040–3061.

Willmott, C.J., C.M. Rowe, and Y. Mintz, 1985: Climatology of the terrestrial seasonal water cycle. *J. Climatology*, **5**, 589–606.

Wurtele, M.G., R.D. Sharman, and T.L. Keller, 1987: Analysis and simulation of a troposphere–stratosphere gravity wave model. Part I. *J. Atmos. Sci.*, **44**, 3269–3281.

Wyser, K., 1998: The effective radius in ice clouds. *J. Climate*, **11**, 1793–1802.

Yoshimura, H. and T. Matsumura, 2004: Semi-Lagrangian Toitsu model. *Report of Numerical Prediction Division*. **50**,

51–60. (in Japanese, *Suuchiyohouka Houkoku Bessatsu*)

Yoshimura, H. and T. Matsumura, 2003: A Semi-Lagrangian Scheme Conservative in the Vertical Direction. *Research Activities in Atmospheric and Ocean Modeling, CAS/JSC Working Group on Numerical Experimentation*, **33**, 0319–0320.

Zhong, W. and J.D. Haigh, 1995: Improved broadband emissivity parameterization for water vapor cooling rate calculations. *J. Atmos. Sci.*, **52**, 124–138.